Geomorphology 295 (2017) 16–27

Contents lists available at ScienceDirect

Geomorphology

journal homepage: www.elsevier.com/locate/geomorph

Self-dissimilar landscapes: Revealing the signature of geologic constraints on landscape dissection via topologic and multi-scale analysis

Mohammad Danesh-Yazdi[a,*], Alejandro Tejedor[b], Efi Foufoula-Georgiou[b]

[a] Department of Civil, Environmental, and Geo-Engineering, St. Anthony Falls Laboratory, National Center for Earth-Surface Dynamics, University of Minnesota, Minneapolis, MN, USA

[b] Department of Civil and Environmental Engineering, University of California, Irvine, CA, USA

ARTICLE INFO

Keywords:
Self-dissimilarity
Landscape topography and river network topology
Wavelet multi-scale analysis and synthesis
Spectral gap

ABSTRACT

Climatic or geologic controls, such as tectonics or glacial drainage, might impose constraints on landscape self-organization resulting in spatial patterns of rivers and valleys which do not obey the typical self-similar relationships found in most landscapes. The goal of this study is to quantify how such geologic constraints express themselves on channel network topology, spatial heterogeneity of drainage patterns, and emergence of preferred scales of landscape dissection. We use as an example a basin located in the Upper Midwestern United States where successive glaciations over the past thousand years have led to a pronounced spatially anisotropic channel network structure which defeats most scaling laws of fluvial landscapes. This is contrasted with another river basin in the North-Central U.S. which has been organized under the absence of major geologic influences and follows a typical self-similar channel network organization. We show how the geologic constraints have imposed a competition for space which is captured in the slope–local drainage density probabilistic structure, in the failure of self-similarity in basin-wide river network topology, and in the length-area scaling relationship being not typical of fluvial landscapes. Via a two-dimensional wavelet analysis and synthesis, we demonstrate the occurrence of a gap in the power spectrum which corresponds to the presence of preferred scales of organization, and characterize them through multi-scale detrending. The developed methodologies can be useful in advancing our geomorphologic understanding of how external controls might manifest themselves in creating a landscape dissection that is outside the norm and how this dissection can be studied objectively for understanding cause and effect.

1. Introduction

Landscape self-organization driven by the movement of water and sediment, and the emergence of river networks that exhibit a hierarchical structure across a range of scales have been the subjects of intensive research over the past decades (e.g., see Rodriguez-Iturbe and Rinaldo, 2001 and references therein). Recently, Zanardo et al. (2013) studied 408 river networks from 50 basins with different geographic location and climate across the United States to assess if the majority of the river networks exhibit self-similarity (SS) in their topological structure. Through a rigorous statistical testing of the Hortonian and Tokunaga self-similarities (see Zanardo et al., 2013 for a detailed representation of these tests), they concluded that 96% of the river networks overwhelmingly exhibited Hortonian Self-Similarity (HSS), while 80% of them followed a topological hierarchical structure that can be characterized successfully by Tokunaga Self-Similarity (TSS). Despite the wealth of studies on landscapes drained by river networks that exhibit HSS, detailed studies of those 20% basins that break the stricter TSS are lacking. The goal of this work is to explore such "outlier basins" which we call "self-dissimilar" and propose methodologies that can probe into their structure in ways that are able to reveal spatially heterogeneous organization and preferential scales of dissection, which then can be related to the underlying controls of, e.g., climate or geology.

Fig. 1a illustrates an example of such basins corresponding to the 43,400 km^2 Minnesota River Basin (MRB) located in the Upper Midwestern Unites States. The geologic history of the MRB (Ojakangas, 1982; Nicollet, 1993) reveals that successive glaciations around 100,000–10,000 BP and the draining of glacial Lake Agassiz in 13,400 BP drastically carved this landscape (Clayton and Moran, 1982; Belmont et al., 2011). While glacial lobes draining over most of this basin left behind a flat and lake-punctuated landscape in the central-

* Corresponding author at: Department of Civil, Environmental, and Geo-Engineering, St. Anthony Falls Laboratory, National Center for Earth-Surface Dynamics, University of Minnesota, Minneapolis, 2 Third Ave SE, Minneapolis, MN 55414-2196, USA.
E-mail address: dane0049@umn.edu (M. Danesh-Yazdi).

http://dx.doi.org/10.1016/j.geomorph.2017.06.009
Received 21 September 2016; Received in revised form 11 June 2017; Accepted 11 June 2017
Available online 21 June 2017
0169-555X/

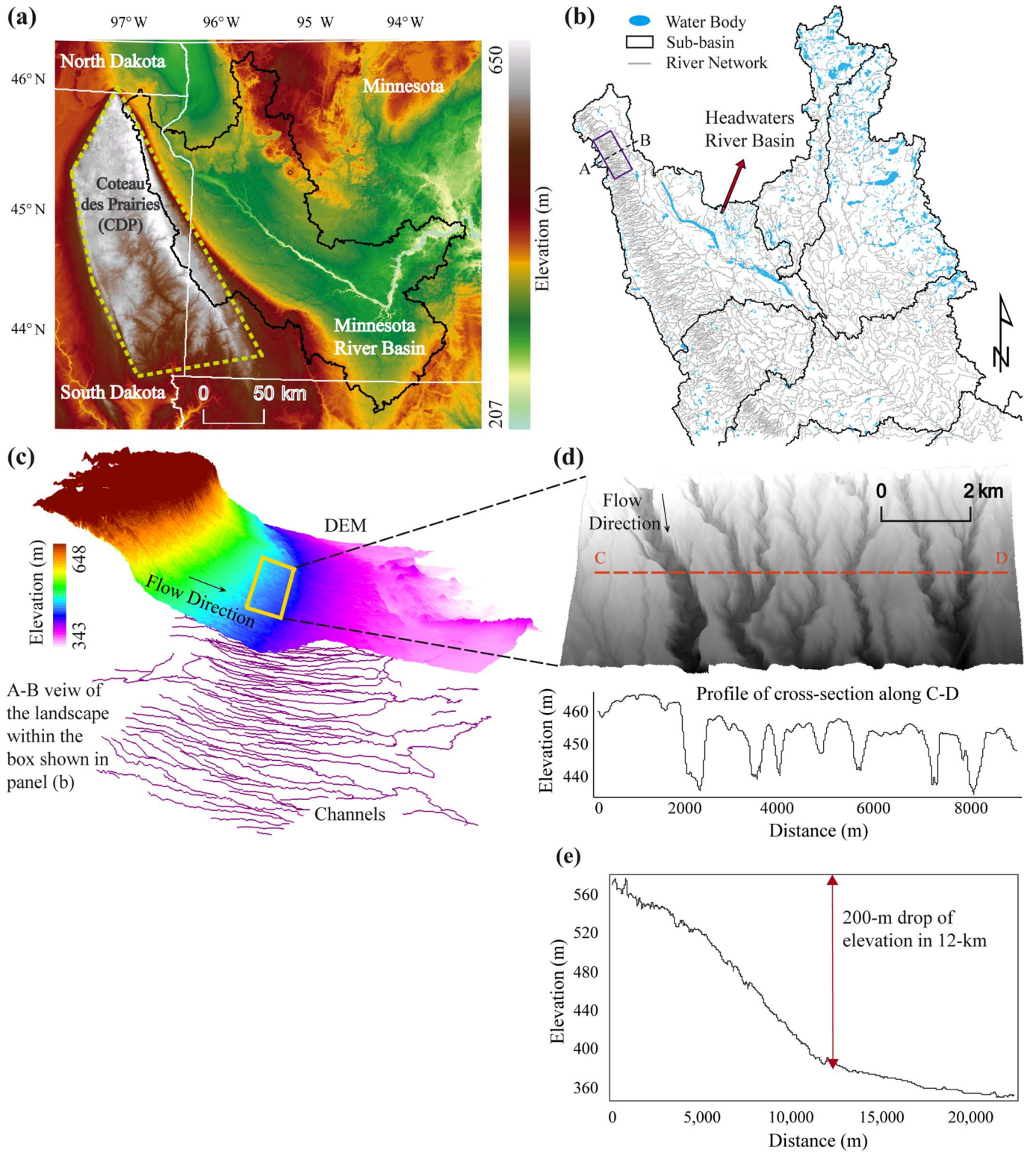

Fig. 1. Illustration of the Minnesota River Basin (MRB) and the Coteau des Prairies (CDP) region. (**a**) Elevation map of the MRB and the CDP residing along the South Dakota border and extending to the Northwestern part of the MRB. (**b**) River network topology of the Northern part of the MRB, including the Headwaters sub-basin which encompasses a portion of the CDP. (**c**) 3D view of the Headwaters landscape delineated by the box shown in (b), showing the presence of a dense number of fairly parallel channels. (**d**) Hillshade of the DEM corresponding to a 70 km^2 patch in the high slope region, depicting quasi-periodic ridges and valleys in this part of the landscape. (**e**) Longitudinal profile of the cross section A–B within the box shown in (b), indicating a 200 m drop in elevation within a 12 km horizontal distance.

eastern part, the western bedrock part was not eroded (Fig. 1b). Instead, repeated glacial cycles covered that bedrock with glacial till deposits and formed the 320 km long, 160 km wide geological feature called Coteau des Prairies (CDP) residing along the South Dakota border and extending to the northwestern part of the MRB. At the edge of the CDP (Fig. 1c,d) there is a pronounced difference in the fluvial dissection compared to the rest of the basin, expressed by the presence of a dense number of steep channels and quasi-periodic ridges and valleys. This high slope region (HSR) includes channels with slope larger than 0.01 m m^{-1} and maximum elevation less than 500 m. A cross-section

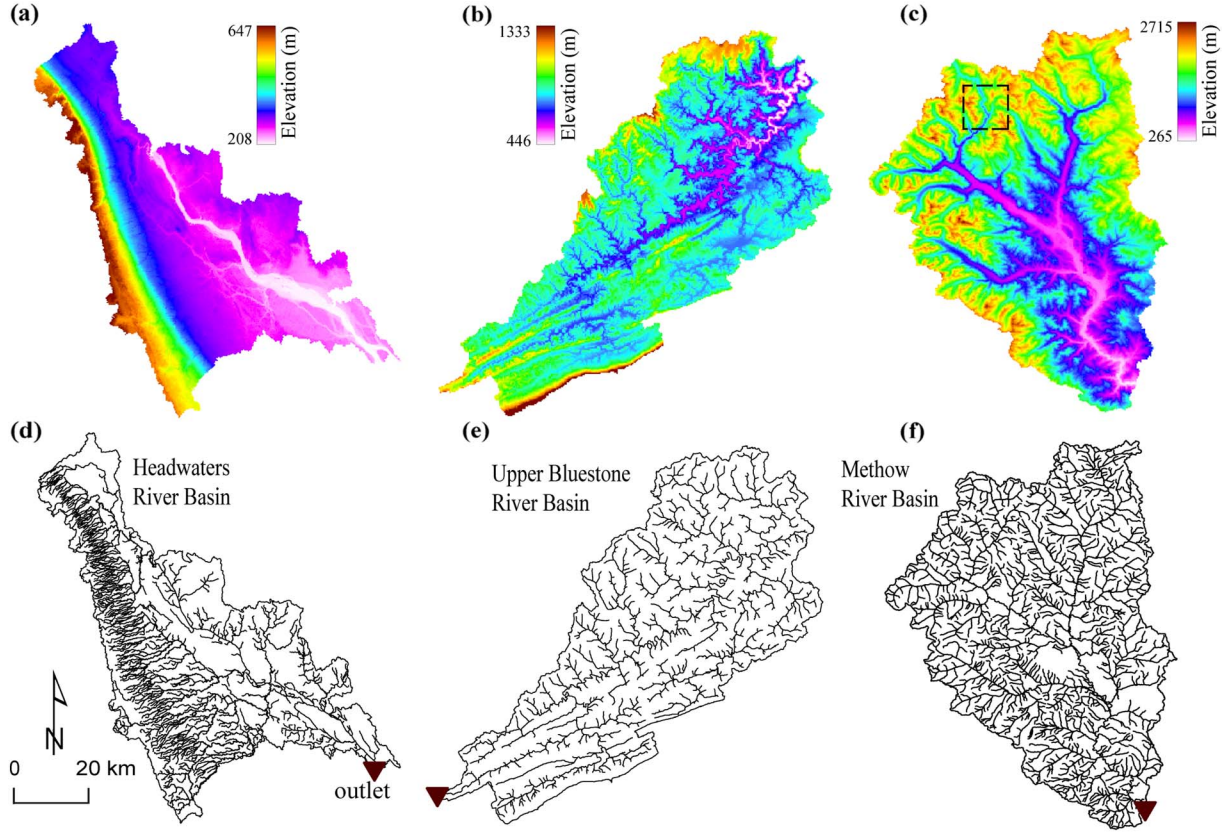

Fig. 2. Digital Elevation Model (DEM) and river network topology of the self-similar Methow and self-dissimilar Headwaters and Upper Bluestone basins. (**a–c**) DEM of the 5400 km^2 Headwaters basin (located in Southwestern Minnesota, U.S.), 1200 km^2 Upper Bluestone basin (a tributary of the much larger New River Basin located in West Virginia, U.S.), and 4900 km^2 Methow basin (located in Northern Washington, U.S.), respectively. (**d–f**) NHDPlus2 (2012) channel network of the Headwaters, Upper Bluestone, and Methow basins, respectively.

of these almost parallel channels in Fig. 1d reveals that these are not rills, but well-formed channels ranging in depth from 10 to 20 m. The longitudinal profile (Fig. 1e) of the analyzed area shown by the box in Fig. 1b and expanded in Fig. 1c shows a 200 m drop in elevation within a 12 km horizontal distance, resulting in the gradient of 0.017 m m^{-1} (see also Gran et al., 2009).

Fig. 2a,d shows the Digital Elevation Model (DEM) and the drainage pattern of the Headwaters River Basin, one of the 12 major sub-basins of the MRB, encompassing a portion of the CDP with a peculiar river network topology, and Fig. 2b,e shows those of the Upper Bluestone River Basin in West Virginia, U.S., as another example of a geologically-controlled landscape. The Upper Bluestone River Basin is a tributary of the much bigger New River Basin, which experienced ten geologic era-periods dividing the basin into three major physiographic provinces, that is, Appalachian Plateaus, Ridge and Valley, and the Blue Ridge Provinces (Paybins, 2000). The Ordovician Taconic Orogeny was the first well-known tectonic event which formed a chain of mountains to the north and east of West Virginia and the next Devonian Acadian Orogeny tectonic event further formed a new set of mountains to the northeast. This strong folding and thrust faulting resulted in the development of long folded ridges which are underlain by sedimentary rocks and separated by relatively flat, broad valleys (Cardwell, 1975).

The above basins are only a few examples of a broader category of geologically-controlled landscapes at which deviation from the universal scaling relationships is recognizable from both the landscape dissection structure and the underlying forming processes. For instance, contrasting relationships were found between specific sediment yield and drainage area across a wide range of spatial scales in various regions of Canada, as compared to the typically observed negative correlation (between specific sediment yield and drainage area), e.g., in the south-eastern United States (e.g., see de Vente et al., 2007 and references therein). These opposing trends have been associated with the activity of rivers that are still responding to large volumes of sediments remobilized during periods of glaciation (e.g., Church and Slaymaker, 1989). In the study of slope-control on the aspect ratio of weakly dissected river basins (~10–10^3 km^2), Castelltort et al. (2009) also attributed anomalous results obtained from some basins in the Columbia River Basin (46° 0′ 0″ N, 116° 0′ 0″ W) to the influence of past tectonics when the North-American plate moved south-west over the Yellowstone Plume.

Although subjected to a different type of control, all the aforementioned basins share communalities of carrying the imprint of external forcing, offering a playground for advancing our geomorphological understanding of cause and effect, studying quantitatively how geologic constrains express themselves on the river network topology, and developing objective methodologies that can explore the spatial heterogeneity and variability of such basins as a function of scale. Addressing these issues constitutes the chief objective of this study. We additionally highlight the morphological differences between self-dissimilar and self-similar landscapes by contrasting the Headwaters River Basin with the 4900 km^2 Methow River Basin (Fig. 2c,f) located in North-Central Washington, which is known to exhibit a typical self-similar channel network organization (Zanardo et al., 2013) and to have reached a geomorphic stable condition (United Stated Bureau of Reclamation, 2008).

To address questions of spatial heterogeneity across different scales and quantify the particular scales and locations contributing mostly to the landscape variability, a localized multi-scale analysis framework, such as that provided by wavelets, is needed. Wavelet analysis has attractive properties such as spatial and spectral localization which allow characterization of differences in the shape and orientation of topographic features in either one or two dimensions (e.g., Booth et al.,

2009; Kalbermatten et al., 2012; Doglioni and Simeone, 2014). Here, we examine the wavelet spectrum to study the distribution of landscape variance across scales. We also apply two-dimensional Discrete Wavelet Transform (DWT) and multi-resolution representation to characterize regular topographic features with preferred scales of organization via a multi-scale landscape detrending.

This paper is organized as follows. In Section 2, landscape dissection analysis is performed through tests of river network SS, probabilistic study of the relationship between the local drainage density and channel slope, and scaling of the length-area relationship. Section 3 demonstrates how wavelet multi-scale analysis and synthesis can be used to identify characteristic scales within a landscape, and Section 4 concludes by summarizing the important findings and suggestions for future research.

2. Landscape dissection analysis

2.1. Tests of Hortonian and Tokunaga self-similarity

If a river network is represented by a tree composed of links (stream channels) and nodes (stream junctions), in the Horton-Strahler ordering scheme: (1) external links or sources have order equal to 1; (2) when links of the same order w join, the order of the immediate downstream link is $w + 1$; and (3) the link directly downstream of two joining links with different orders is labeled with the highest order of the two (Horton, 1945; Strahler, 1957). The order (Ω) of a finite river network is equal to the maximum order of links present in the network. For a Hortonian self-similar river network, $N_w / N_{w+1} = R_B$, where R_B is the so-called bifurcation ratio, and N_w is the number of branches of order w, where branches are defined as connected links of the same order. Other commonly studied Horton laws also apply in terms of the average length and average upstream contributing area of the braches of order w, but are not considered here.

The Tokunaga indexing accounts for the side branching structure of a river network, i.e., if N_{ij} is the number of branches of order i that join a branch of order j, and N_j is the total number of branches of order j, the Tokunaga index T_{ij} is defined as $T_{ij} = N_{ij} / N_j$. Thus T_{ij} can be interpreted as the average number of branches of order i that join a branch of order j. If $\tau_{ij}^{(l)}$ $(1 \le l \le N_j,\ 1 \le i < j \le \Omega)$ denotes the number of branches of order i that join the nonterminal nodes of the l-th branch of order $j > i$, a tree is called self-similar if its side-branching structure is the same for all branches of the same order (i.e., $\tau_{ij}^{(l)} = T_{ij}$, $1 \le l \le N_j$, $1 \le i < j \le \Omega$) and is also independent of the branch order (i.e., $T_{i(i+k)} = T_k$, $2 \le i + k \le \Omega$). The TSS applies an extra constraint (Tokunaga, 1978) based on which the ratio of two consecutive Tokunaga indices is constant, i.e., $T_{k+1} / T_k = c$, $1 \le k \le \Omega - 1$. This gives rise to a family of trees represented by $T_k = ac^{k-1}$, where the positive parameters a and c are indicative of the first-order side-branching (T_1) and the degree of higher order branching, respectively.

River networks for the Headwaters and Methow basins were obtained from the National Hydrography Dataset (NHDPlus 2.10 released in 2012) and are shown in Fig. 3a and b, respectively. Fig. 3c and d show the Horton law of the number of branches, giving the bifurcation ratio equal to 2.87 and 3.93 for the Headwaters and Methow basins, respectively. The linear relationships with coefficients of determination (R^2) equal to 0.92 and 0.98 are both statistically significant, implying that both river networks follow the HSS. However, two points are worth noting. First, although even visually the Headwaters basin exhibits distinct scales of topologic variability not homogeneously present in the landscape, the Hortonian analysis (which essentially applies a coarsening of the landscape based on basin order) is blind to such a structure and indicates the presence of SS. The inability of the Hortonian analysis to critically depict deviations from SS has also been reported in other studies (e.g., Kirkby, 1976; Gupta and Waymire, 1989; Kirchner, 1993; Tarboton, 1996). Second, we note that the estimated bifurcation ratio of 2.87 for the Headwaters basin is very low compared to that expected for typical river networks (~4), raising suspicion in its interpretation. The reason for this deviation might be tracked back by comparing the real number of branches of different orders in this basin to the ones "expected" from the bifurcation ratio of 2.87. Indeed, since the maximum order of the Headwaters basin is 7, it is expected that the network includes approximately three branches of order 6, eight branches of order 5, …, 195 branches of order 2, and 559 branches of order 1 if we assume it maintains the bifurcation ratio throughout the lower-order branches. However, topologic analysis of this river network reveals that there exists a lower number of streams with orders 2 to 5, but a much larger number of first-order streams (648) than expected. Fig. 3a shows that the vast majority of such first-order streams not only is present in the high slope region (HSR) of the CDP, but also these streams drain almost parallel to each other decreasing the chance to join and create higher order streams, which ultimately results in a smaller bifurcation ratio than expected for typical landscapes.

Fig. 3e and f show the Tokunaga index against the side-branching order for the Headwaters and Methow basins, respectively. It is clearly seen how the stricter TSS is violated in the Headwaters basin, but not in the Methow basin. This is because the TSS considers not only the first-order organization (i.e., number of branches of order w draining into branches of order $w + 1$, that is, $N_{w,w+1}$), but also the transition probability of a branch of order w to drain into a branch of order $w + k$, implying higher order branching. It was found that the total number of low order side-branchings (i.e., N_{12}, N_{23}, N_{34}, N_{13}, N_{24}, N_{14}), which are essentially all the existing transitions in the HSR, forms nearly 60% of the same transitions present within the whole basin. This indicates how the hierarchical progression from one order to another is overwhelmingly violated at the above transitions, probing further examination of the causes of the abundance of lower order side-branching within the HSR. Indeed, steep facies (or knickzones) created by the geologic forcing in this region have maintained large areas of low convergence inhibiting the merging of streams to higher orders and resulting in a large number of low order channels within the HSR. This observation is further investigated in the next section by studying the local drainage density and other geomorphic attributes of the landscape.

2.2. Slope–local drainage density analysis

Drainage density, which is a measure of how dense a landscape is dissected by fluvial channels, has been the focus of several studies aiming to understand how dissection is controlled by factors related to climate and relief (e.g., Tucker and Bras, 1998 and references therein). Since drainage density in its global form (defined as the total length of fluvial channels divided by total drainage area) cannot account for spatial heterogeneities in a landscape, we compute here the *local drainage density* (*LDD*), defined as the ratio of the length of a channel to the incremental contributing area draining directly into that channel. Based on this definition, Fig. 4a–d illustrates the color mapping of *LDD* as well as the channel slope (S) on the river network of the Headwaters and Methow basins.

First, it is observed that although the local slopes in the Headwaters basin are on average smaller than those in the Methow basin (average slope of $0.009\ \mathrm{m\,m^{-1}}$ vs. $0.129\ \mathrm{m\,m^{-1}}$, respectively), a reversal is found for *LDD* values (average *LDD* of $1.49\ \mathrm{km\,km^{-2}}$ vs. $1.02\ \mathrm{km\,km^{-2}}$, respectively). The maximum *LDD* value in the Headwaters basin ($4.98\ \mathrm{km\,km^{-2}}$) is also twice as large as the maximum *LDD* value in the Methow basin ($2.49\ \mathrm{km\,km^{-2}}$), implying that *LDD* does not necessarily increase with the local slope (see Table 1 for other statistics on the channel slope and *LDD*). This is counterintuitive as one expects steeper slopes to create longer and narrower incremental areas due to less flow convergence; however, the deviation found here can be an indicator of large-scale heterogeneities in the landscape imposed by geologic controls (e.g., Castelltort and Simpson, 2006; Castelltort et al., 2009). Second, higher *LDD* values in the Headwaters

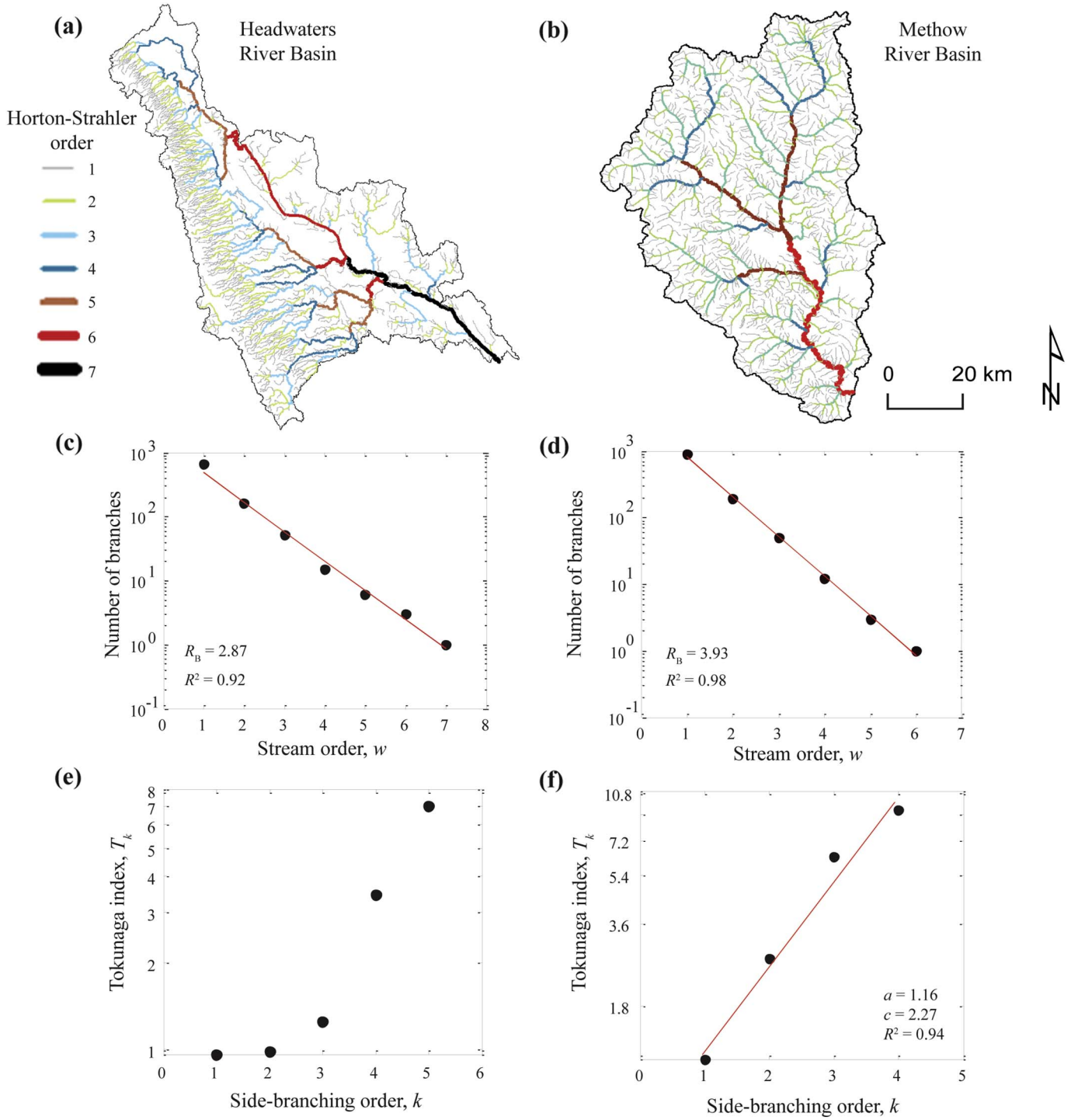

Fig. 3. Topology and tests of self-similarity (SS) for the river networks of the Headwaters and Methow basins. (**a**) and (**b**) show the channel network colored by the Horton-Strahler order in the Headwaters and Methow basin, respectively. (**c**) and (**d**) depict the Hortonian scaling for the number of branches, confirming the Hortonian self-similarity (HSS) for both river networks. (**e**) and (**f**) show the Tokunaga index versus side-branching order, revealing that the stricter Tokunaga self-similarity (TSS) is violated in the Headwaters basin, but not in the Methow basin.

basin are concentrated in the HSR which is very steep and dissected by low order channels (up to order 3), while the Methow basin shows a spatially uniform distribution of slope and *LDD* values. A functional comparison of slope and *LDD*, as shown in Fig. 4e, further confirms that in the Headwaters river basin high values of *LDD* and slope fall in the same topographic region related to the HSR, while this is clearly not true in the Methow basin where channels with high *LDD* do not necessarily correspond to high slopes but span a relatively wide range of slopes. These observations underscore not only the subtle differences between the Headwaters and Methow basins with respect to their landscape organization, but also highlight how the Headwaters basin's HSR has experienced a completely different dissection mechanism compared to the rest of the basin. Fig. 4f quantifies this by showing the scaling relationship between the channel length and incremental drainage area for all the channels within and outside of the HSR. The high scaling exponent of 0.70 for the HSR affirms the presence of longer streams and narrower contributing areas in this region, demonstrating the particular type of dissection formed in this part of the landscape.

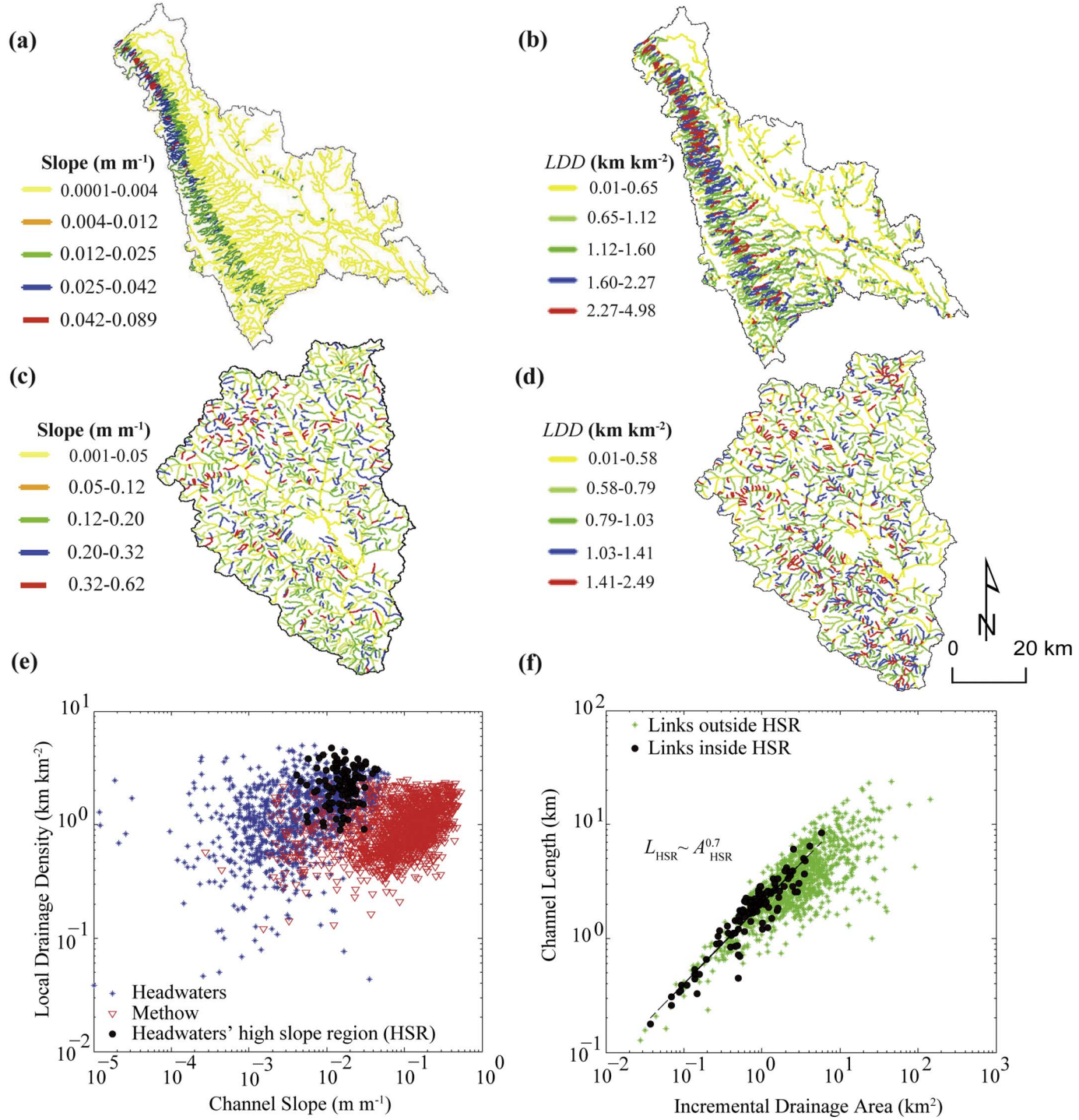

Fig. 4. Channel slope and local drainage density (*LDD*) spatial distribution, and their functional relationship. (**a and b**) Spatial distribution of channel slope and *LDD* in the Headwaters basin, showing concentration of high *LDD* in the high slope region (HSR) with steep channels. (**c and d**) Depicts a uniform spatial distribution of channel slope and *LDD* in the Methow basin. (**e**) Functional comparison of the channel slope and *LDD* between the Headwaters (blue stars), the Methow (red triangles), and the HSR (black circles). (**f**) Scaling relationship between channel length and incremental drainage area in the Headwaters basin. (For interpretation of the references to color in this figure legend, the reader is referred to the web version of this article.)

To probe further into the relationship between *LDD* and local slope and specifically to investigate how this relationship might change in a magnitude–frequency space under the presence of spatial heterogeneity, the joint probabilistic structure of these two attributes is studied. Fig. 5c,d shows the quantile–quantile (Q–Q) plots of *LDD* and slope for the Headwaters and Methow basins, while Fig. 5a,b shows the marginal probability distributions functions (PDFs). In the Methow basin, the *LDD* and slope PDFs follow each other up to the 92nd quantile after which the tails of the two distributions diverge as evidenced by their deviation from the line passing through the 25th and 75th quantiles. However, this breaking point (corresponding to S^* and LDD^*) for the Headwaters basin takes place at the 76th quantile, indicating that higher slopes do not necessarily support higher *LDD* values. The position of all channels with *LDD* and slope beyond the Q–Q plot's breakpoint are mapped on the Headwaters and Methow river networks as depicted in Fig. 5e and f, respectively. It is seen that these

Table 1
Statistics of the channel slope (*S*) and local drainage density (*LDD*) in the Headwaters and Methow River Basins.

Attribute	Statistic	Headwaters basin	Methow basin
Channel slope (*S*)	Mean ($m\ m^{-1}$)	0.009	0.129
	Standard deviation ($m\ m^{-1}$)	0.011	0.102
	Skewness coefficient	1.82	1.17
	Maximum ($m\ m^{-1}$)	0.089	0.620
Local drainage density (*LDD*)	Mean ($km\ km^{-2}$)	1.49	1.02
	Standard deviation ($km\ km^{-2}$)	0.89	0.46
	Skewness coefficient	0.88	0.73
	Maximum ($km\ km^{-2}$)	4.98	2.49

channels are located throughout the Methow basin while they are concentrated within the HSR in the Headwaters basin. Indeed, the western part of the Headwaters landscape has been confined in space creating competition for the developing channels, resulting in the formation of long and fairly parallel low-order channels. Such a preferential dissection and reduced *LDD* variability at small spatial scales once again is a signature of the strong influence of external forcings, geologic control in this basin, on the landscape organization, leading to deviation from the typical relationships under SS. It is interesting to report that the same analysis performed on the Bluestone River Basin showed a breakpoint of the Q–Q plot of the *LDD*–Slope at approximately the same 75th quantile. Although we are far from making a general conclusion about the quantile of the occurring breakpoint for self-dissimilar landscapes, it is apparent that this Q–Q plot can serve as an indicator of deviation from SS and the presence of heterogeneity in the spatial organization of a landscape. Our next goal is to quantify spatial scales of preferred dissection for which we need appropriate tools such as localized decomposition to interrogate the landscape locally. This issue is examined in the next section.

3. Landscape multi-scale analysis and preferred scales of organization

Multi-scale filtering of landscapes for isolating features within a desired range of scales can be achieved by spectral analysis via Fourier Transform (FT) or Wavelet Transform (WT). Both the FT and the WT perform a convolution of the landscape topography with a family of functions, that is, the sine and cosine functions for the FT and the wavelet functions for the WT. In spite of the widespread application of the FT to study topographic data (e.g., Ansoult, 1989; Hough, 1989; Cheng et al., 2000; Wörman et al., 2007; Perron et al., 2008; Orloff et al., 2013), its disadvantages include the lack of spatial localization and the prerequisite for parametric removal of large-scale trends or non-stationarities in the data before the FT can be applied. Instead, the WT is a localized transform in space and frequency and allows for the non-parametric removal of trends by appropriate selection of the mother wavelet (Foufoula-Georgiou and Kumar, 1994; Mallat, 1989a,b).

The WT of a signal $f(t)$ is defined as

$$\mathrm{WT}f(\lambda,b) = < f(t), \psi^*_{\lambda,b}(t) > = \int_{-\infty}^{+\infty} f(t)\psi^*_{\lambda,b}dt \tag{1}$$

where $< \cdot,\cdot >$ denotes the inner product (convolution) of $f(t)$ with a family of functions $\psi^*_{\lambda,b}(t)$ which are the complex conjugates of the wavelet function $\psi_{\lambda,b}(t)$, expressed as

$$\psi_{\lambda,b}(t) = \frac{1}{\sqrt{\lambda}}\psi\left(\frac{t-b}{\lambda}\right), \quad \lambda > 0 \tag{2}$$

where λ is the scale and b is the location parameter controlling the contraction (or dilation) and translation of the mother wavelet $\psi(t)$, respectively. A wavelet function has zero mean, i.e., $\int_{-\infty}^{+\infty} \psi(t)dt = 0$, and higher order moments may also be zero, $\int_{-\infty}^{+\infty} t^k\psi(t)dt = 0,\ k = 0, ...,N-1$, allowing removal of polynomial trends up to degree N.

3.1. Quantifying preferred scales of organization

The wavelet power spectrum (WPS) of topography measures how the variance of the topography is distributed across scales. Contrary to the Fourier spectrum, it offers the advantage of non-parametric surface detrending and also minimizing aliases via the space-frequency localization property of wavelets (Mallat, 1989a,b). Here we use the Mexican hat wavelet (which has two zero moments and thus removes polynomial trends of order 2) to compute the continuous WPS. Indeed, the power spectrum (PS) can be computed across continuous fine scales via the Continuous Wavelet Transform (CWT), while the dyadic (i.e., power of two) scales in the orthogonal DWT limits the WPS to some definite discrete scales (depending on the size of the data) making it harder to interpret possible abrupt changes in the distribution of energy across scales. A number of past studies have reported that the topography is typically scale-invariant and the PS obeys a single power-law scaling relationship with frequency (f) according to $PS(f) \propto f^{-\beta}$ (e.g., Pelletier, 1999; Veneziano and Iacobellis, 1999; Gagnon et al., 2006). Since the amplitude and the wavelength of topographic features are related to the *PS* and f, respectively, the spectral slope (β) indicates how the height-to-width ratio of landforms varies with scale. In general, the spectral slope of a self-similar topography computed from a two-dimensional spectrum is equal to 3 (i.e., the landforms' height-to-width ratio is independent of scale), while topographies with constant β other than 3 are categorized as self-affine (e.g., Voss, 1988).

Fig. 6a and b show the WPS of the landscape topographies corresponding to a 70 km^2 patch in the Headwaters basin's HSR (Fig. 1c,d) and a 190 km^2 patch extracted from the Methow basin (marked by the box in Fig. 2c), respectively. The WPS of the patch of Methow gives a single spectral slope equal to 2.2 indicating that the landscape topography is self-affine and obeys the same scaling relationship across a range of scales. However, in the Headwaters' WPS, there are two different scaling regimes with spectral slopes equal to 4.9 and 2.1, separated by a spectral gap between the scales of 0.3 and 1.5 km. The larger spectral slope above the spectral gap implies that large-scale features (i.e., scales larger than 1.5 km) have larger height-to-width ratios compared to small-scale features. The spectral gap within a range of scales indicates an energy plateau which signifies that these scales contribute more to the overall energy (or variance of the topography) as compared to the case where the spectrum maintained a constant slope within the whole range of scales; it indeed documents the existence of regular topographic features and some preferred scales of organization. Such features correspond to mildly convergent (almost parallel) channels in the Headwaters basin's HSR, and the profile of a cross-section in this region shown in Fig. 1d confirms that the scales corresponding to the spectral gap (0.3 to 1.5 km) pertain to the distance between the quasi-periodic ridges and valleys in the HSR. The emergence of a spectral gap, and the presence of two distinctly different scaling regimes around it, is viewed as a signature of "a structured self-dissimilarity" in such landscapes providing information about specific scales of preferred organization and probing the question of understanding the processes that lead to such organization across scales. Topographies that exhibit a break in their power spectra have been reported before, as for example in Perron et al. (2008), but landscapes that exhibit a spectral gap over a range of scales have not been reported before to the best of our knowledge.

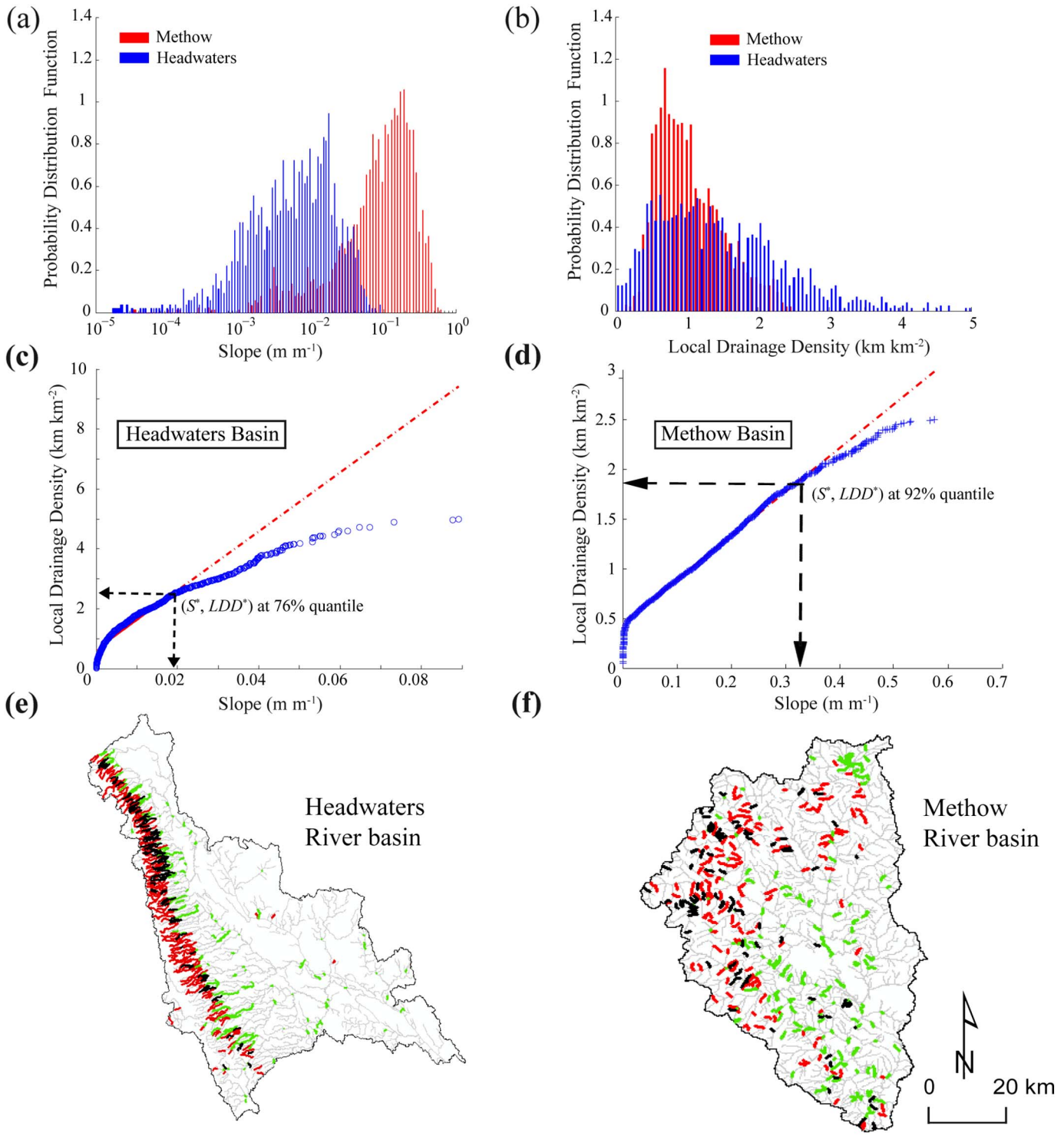

Fig. 5. Probabilistic comparison of the channel slope and local drainage density (*LDD*) in the Headwaters and Methow basins. (**a**) and (**b**) give the channel slope and *LDD* probability distribution function, respectively. (**c**) and (**d**) show the quantile-quantile plots of *LDD* versus slope for the Headwaters and Methow basins, respectively. In panels (**e**) and (**f**), green channels have slope larger than S^*, red channels have *LDD* larger than LDD^*, and black channels are those having both slope larger than S^* and *LDD* larger than LDD^*. Concentration of these channels in the Headwaters' high slope region (HSR) is apparent, while they are distributed throughout the Methow basin. (For interpretation of the references to color in this figure legend, the reader is referred to the web version of this article.)

3.2. Characterizing landscape regularity via multi-scale detrending

Although for multi-scale analysis of landscapes the continuous wavelet transform is appropriate, for landscape detrending and reconstruction of local features of interest, a DWT is necessary. The discrete wavelet function can be constructed by discretizing the scale and location parameters (usually in a logarithmic scale) written as

$$\psi_{m,n}(t) = \frac{1}{\sqrt{\lambda_0{}^m}}\psi\left(\frac{t - nb_0\lambda_0{}^m}{\lambda_0{}^m}\right) \tag{3}$$

where m and n are non-zero integers, λ_0 is a fixed value greater than 1, and b_0 is a positive value. The convolution of signal $f(t)$ with $\psi_{m,n}(t)$ is called the DWT.

By choosing $\lambda_0 = 2$ and $b_0 = 1$ (called dyadic grid discretization), a

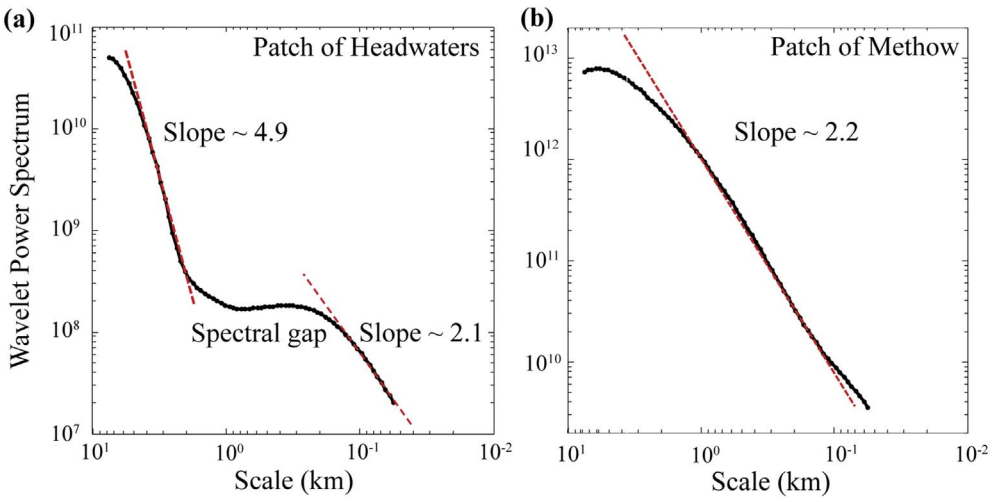

Fig. 6. Wavelet power spectra. (**a**) and (**b**) depict the wavelet power spectrum (WPS) for the patch of Headwaters (Fig. 1d) and the patch of Methow (Fig. 2c) basins, respectively. The WPS of the patch of Methow shows a single scaling regime with exponent equal to 2.2 denoting the self-affinity of this landscape. However, the WPS of the patch of Headwaters shows two scaling regimes separated by a spectral gap between scales ~0.30 and 1.50 km.

certain class of wavelets $\psi(t)$ can be constructed such that $\psi_{m,n}(t)$ are orthogonal to their dilations and translations (i.e., $< \psi_{m,n}(t), \psi_{m',n'}(t) > = \delta_{m,m'}\delta_{n,n'}$, where δ_{ij} is the Kronecker delta function) and form a complete orthonormal basis for all signals that have finite energy. Such signals $f(t)$ can then be written as a linear combination of the wavelets $\psi_{m,n}(t)$, i.e.,

$$f(t) = \sum_{m=-\infty}^{+\infty} \sum_{n=-\infty}^{+\infty} < f(t), \psi_{m,n}(t) > \psi_{m,n}(t) \tag{4}$$

where the weights are the inner products of $f(t)$ with the corresponding wavelet function $\psi_{m,n}(t)$. Mallat (1989a, b) showed that there exists a unique function $\varphi(t)$ with certain properties, called the *scaling function*, such that $f(t)$ can also be written as

$$f(t) = \sum_{n=-\infty}^{+\infty} < f(t), \varphi_{m_0,n}(t) > \varphi_{m_0,n}(t) + \sum_{m=-\infty}^{m_0} \sum_{n=-\infty}^{+\infty} < f(t), \psi_{m,n}(t) > \psi_{m,n}(t) \tag{5}$$

where the first term in the RHS represents the average or approximation of $f(t)$ at scale m_0 and the second term captures all the "details" of $f(t)$ at scales equal and smaller than m_0. It can be easily shown from the above equation that the following recursive equation results:

$$\tilde{f}_{m-1}(t) = \tilde{f}_m(t) + f'_m(t) \tag{6}$$

implying that a signal approximation at scale $m-1$, $\tilde{f}_{m-1}(t)$, can be written as the sum of the signal approximation at the immediately smaller scale m, $\tilde{f}_m(t)$, plus its detail at that scale, $f_m'(t)$.

Eq. (6) constitutes the so-called wavelet multi-resolution representation (Mallat, 1989a). Multi-resolution representation allows for detrending a landscape through the inverse DWT by successive elimination of large-scale features from the topography to better characterize the complex hierarchy of topographic features. From here on, a detrended landscape is denoted by $H_m(t, s)$ and is obtained by setting the approximation coefficients at scale m equal to zero in the reconstruction operation. Fig. 7 schematically shows the general procedure for the multi-resolution decomposition and detrending of a landscape in two dimensions. To analyze two-dimensional topographic data such as DEMs, two-dimensional orthonormal bases can be constructed by taking the tensor product of the one-dimensional scaling and wavelet bases given above (Mallat, 1989a). If the bandpass center frequency of the chosen mother wavelet is f_c, and the data sampling period (which is the resolution of the DEM) is denoted by Δ, the physical scale (L_m) relating to the scale m is computed by using the following relationship.

$$L_m = \frac{2^m \cdot \Delta}{f_c} \tag{7}$$

The simplest and most widely used discrete orthonormal wavelet is the Haar wavelet which is, however, poorly localized in frequency. Instead, the Daubechies wavelets (Daubechies, 1988, 1992) have enhanced localization in the frequency domain and allow for removal of high order polynomial trends as needed. We chose the most suitable wavelet for our analysis by testing different Daubechies wavelets, i.e., DB1, DB2, …, DB10 on the two patches within the Headwaters and Methow basins (the same patches shown in Figs. 1d and 2c and used in Section 3.1). The best wavelet would be the one that results in the minimum least squares difference between the original landscape and the detrended landscape containing the approximation coefficients at the largest scale, which capture the spatial trend in topography. We found DB5 as the best wavelet for both landscapes with respect to our criterion as it provided a balance between removal of trends and efficiency in the spatial localization compared to other wavelets.

Since the signature of geological controls on landscape organization is embedded in nested topographical features with different spatial scales, multi-scale detrending facilitates reconstructing a portion of the landscape possessing features with certain spatial scales. For instance, the structure of regular features identified by the spectral gap can be spatially located and statistically characterized by successively filtering out the larger scale features from the landscape. Fig. 8a and b show the elevation probability distributions of the detrended landscapes ($H_m(t, s)$, $m = 1, \ldots, 8$) for the Headwaters and Methow patches, respectively. The common observation is that by gradual removal of large scale features, i.e., setting the corresponding wavelet coefficients equal to zero, the elevation probability distribution becomes smoother and more symmetrical. However, the shape of the probability distributions from one level of detrending to another does not change similarly in the patches. Indeed, if the variance of the probability distributions is plotted against scale (Fig. 8c,d), the variability changes proportionally across spatial scales in the patch of Methow (as expected for self-similar landscapes), while the variance of the probability distributions does not change significantly by filtering out the features with wavelengths between 0.36 and 1.44 km from the patch of Headwaters basin. Fig. 8e further depicts the structure of the detrended landscape, $H_4(t, s)$, containing all topographic features with spatial scale equal and less than 0.72 km. The regularity of the features is apparent in this detrended landscape, which corresponds to the quasi-periodic ridges and valleys in the Headwaters basin's HSR and their wavelengths are consistent with the scales already revealed by the spectral gap in the WPS of this landscape.

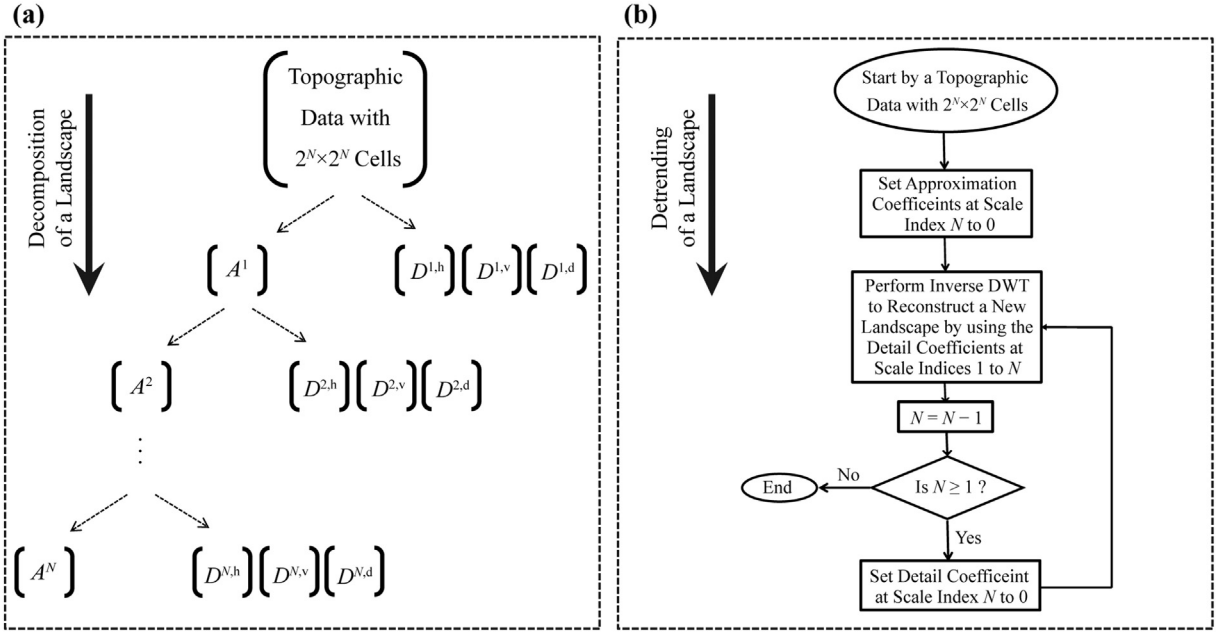

Fig. 7. General procedure for the wavelet decomposition and detrending of a landscape. (**a**) Schematic diagram of the multi-resolution representation of a landscape using two-dimensional discrete wavelet transform (DWT). A^i, $D^{i,h}$, $D^{i,v}$, and $D^{i,d}$, $i = 1, \ldots, N$, are the approximation, horizontal detail, vertical detail, and diagonal detail matrices at scale i, respectively. (**b**) Flowchart of the multi-scale detrending of a landscape using two-dimensional DWT. The detrending procedure starts by setting the approximation coefficients at the largest scale to 0. In the next iterations, the detail coefficients from large to smaller scales are successively set to 0, until all the details are removed from the landscape.

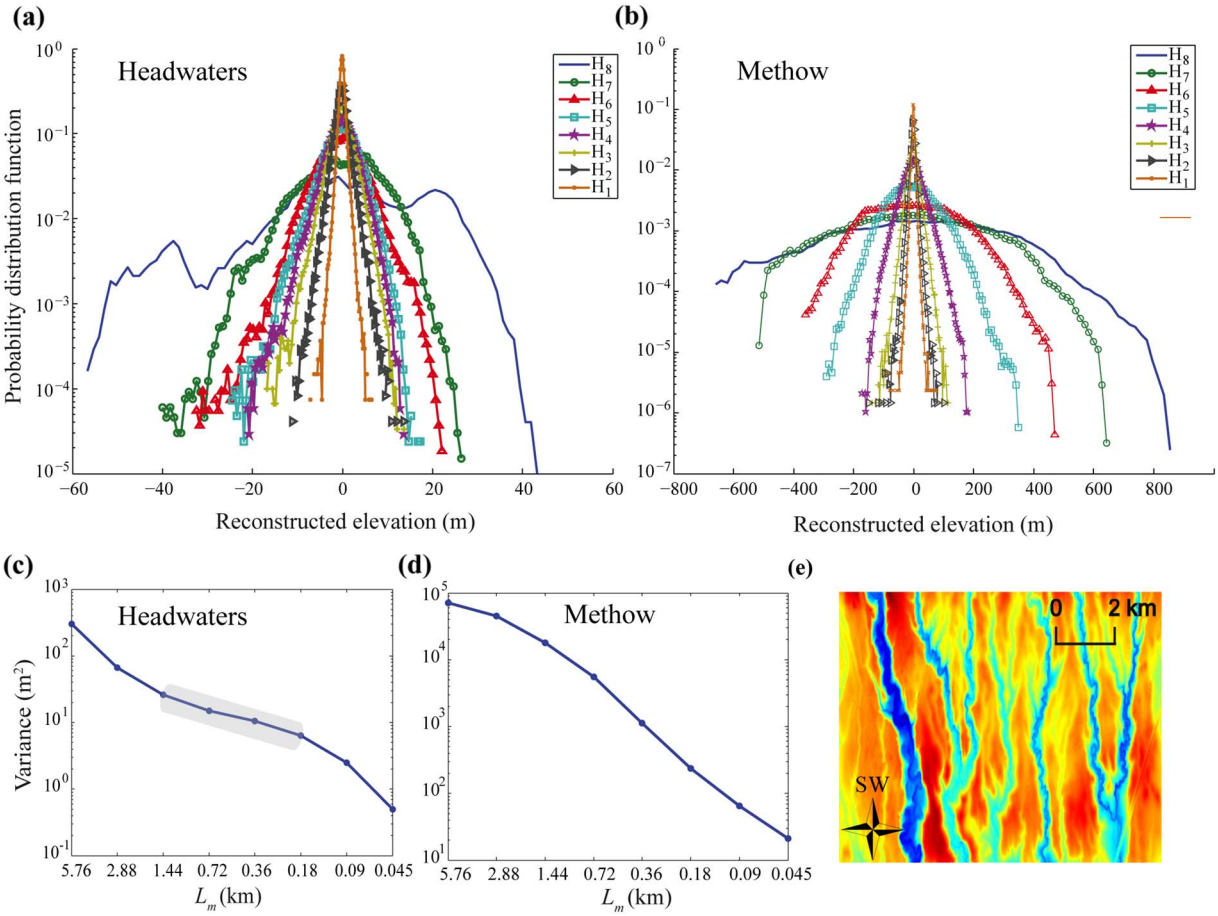

Fig. 8. Elevation probability distribution and the variance of detrended landscapes against scale. (**a and b**) Probability distribution of the detrended landscapes for the patch of Headwaters and Methow basins, respectively. (**c and d**) Variance of the detrended landscapes, $H_m(t, s)$, against scale, L_m. The horizontal axis in these plots gives the largest scale present in $H_m(t, s)$. (**e**) Image view of the detrended landscape, $H4(t, s)$, from the patch of Headwaters basin, showing regularity that corresponds to the quasi-periodic ridges and valleys in the Headwaters' high slope region (HSR).

4. Conclusions

Landscapes possess a hierarchical variability over a wide range of scales: from hillslopes to valleys, and to nested river basins of increasing order. If the physical processes that sculpted a landscape are spatially homogeneous, then it is expected that some kind of order in how this variability changes with scale will be found. In fact, a considerable body of work has centered over the past three decades on quantifying SS in landscape dissection (e.g., see Rodriguez-Iturbe and Rinaldo, 2001). However, if geologically or geomorphologically spatially heterogeneous processes dominated the landscape evolution, one would expect that this heterogeneity will be reflected over some range of scales which would exhibit different spatial organization and variability than other scales. The purpose of this study was to examine landscapes which exhibit spatial heterogeneity in their dissection, and via localized analysis and synthesis identify and quantify scales of preferred organization and relate them to the underlying geologic controls. We call these landscapes "self-dissimilar" and suggest that research is needed to both theoretically characterize these landscapes and to connect their structure to the underlying climatic, tectonic, or geologic mechanisms that have broken the typical symmetries that most landscapes possess. From the analysis presented here, the following conclusions are made:

1) Even in basins which exhibit visually distinct spatially heterogeneous river branching structures, HSS analysis is unable to capture broken symmetries in network topology. However, the stricter TSS analysis can detect the presence of hierarchical irregularities in the branching structure of the river networks.
2) The probabilistic dependence of local slope and *LDD*, examined via a quantile-quantile analysis, has the potential to quantify spatial heterogeneities in landscape dissection by a disproportional lack of high *LDD* at high slopes. Such an analysis is easy to perform and can be a first step in detecting spatial heterogeneities in landscape dissection, which then can be explicitly positioned on the landscape to study cause and effect.
3) The presence of a spectral gap (no net decrease in energy with decreasing scale) in WPS can reveal scales at which excess regularity is present, as for example in the quasi-periodic ridges and valleys, in our case.
4) Using appropriate localized multi-scale filters, the structure of these regular features can be quantified via localized multi-scale detrending by successive removal of features from the largest to the smallest scale of interest.

The analysis presented herein highlighted the need to develop formal methods for studying spatially heterogeneous landscapes in order to understand their drainage structure and relate it to the underlying causative mechanisms. A detailed spatial and spectral interrogation of a landscape as presented herein to detect specific scales and relating them to certain terrain features cannot be achieved by only studying the landscape DEM and geomorphometric attributes, e.g., slope, aspect, and curvature, as these do not provide information about the landscape hierarchical structure. Our study is but one example of demonstrating how the joint landscape decomposition and detrending via the two-dimensional DWT allows for identifying, mapping, and correlating the spatial patterns of DEM to particular geologic structures. Other potential applications of such a framework include, but not limited to, automatic extraction of deep-seated landslides (Kalbermatten et al., 2012; Doglioni and Simeone, 2013) and characterizing their morphologic features such as topography, hummocky, and scarps (Booth et al., 2009), separating erosional features from the landform of a volcano as well as retrieving volcanic activity from topography (Gomez, 2012), and investigating the periodicity and spatial pattern of lineaments associated with tectonic faults (Jordan and Schott, 2005).

Acknowledgments

This research was funded by NSF grant EAR-1209402 under the Water Sustainability and Climate Program (WSC): REACH (REsilience under Accelerated CHange) and benefited from collaborations made possible by NSF grants EAR-1242458 (LIFE: Linked Institutions for Future Earth) and EAR-1342944. The second author acknowledges financial support from the National Center for Earth-surface Dynamics 2 (NSF grant EAR-1246761) postdoctoral fellowship. The third author also acknowledges support provided by the Joseph T. and Rose S. Ling endowed chair.

References

Ansoult, M.M., 1989. Circular sampling for Fourier analysis of digital terrain data. Math. Geol. 21, 401–410. http://dx.doi.org/10.1007/BF00897325.
Belmont, P., Gran, K.B., Schottler, S.P., Wilcock, P.R., Day, S.S., Jennings, C., Lauer, J.W., Viparelli, E., Willenbring, J.K., Engstrom, D.R., Parker, G., 2011. Large shift in source of fine sediment in the Upper Mississippi River. Environ. Sci. Technol. 45, 8804–8810. http://dx.doi.org/10.1021/es2019109.
Booth, A.M., Roering, J.J., Perron, J.T., 2009. Automated landslide mapping using spectral analysis and high-resolution topographic data: Puget Sound lowlands, Washington, and Portland Hills, Oregon. Geomorphology 109, 132–147. http://dx.doi.org/10.1016/j.geomorph.2009.02.027.
Cardwell, D.H., 1975. Geologic History of West Virginia. Vol. 10 West Virginia Geological and Economic Survey.
Castelltort, S., Simpson, G., 2006. River spacing and drainage network growth in widening mountain ranges: river spacing and drainage network growth. Basin Res. 18, 267–276. http://dx.doi.org/10.1111/j.1365-2117.2006.00293.x.
Castelltort, S., Simpson, G., Darrioulat, A., 2009. Slope-control on the aspect ratio of river basins. Terra Nova 21, 265–270. http://dx.doi.org/10.1111/j.1365-3121.2009.00880.x.
Cheng, Q., Xu, Y., Grunsky, E., 2000. Integrated spatial and spectrum method for geochemical anomaly separation. Nat. Resour. Res. 9 (1), 43–52.
Church, M., Slaymaker, O., 1989. Disequilibrium of Holocene sediment yield in glaciated British Columbia. Nature 337 (6206), 452–454.
Clayton, L., Moran, S.R., 1982. Chronology of late Wisconsinan glaciation in middle North America. Quat. Sci. Rev. 1 (1), 55–82.
Daubechies, I., 1988. Orthonormal bases of compactly supported wavelets. Commun. Pure Appl. Math. 41, 909–996. http://dx.doi.org/10.1002/cpa.3160410705.
Daubechies, I., 1992. Ten Lectures on Wavelets. Vol. 61 of CBMS-NSF Regional Conference Series in Applied Mathematics.
Doglioni, A., Simeone, V., 2013. Quantitative geomorphological analysis based on wavelet transforms. In: Margottini, C., Canuti, P., Sassa, K. (Eds.), Landslide Science and Practice. Springer, Berlin Heidelberg, Berlin, Heidelberg, pp. 257–264.
Doglioni, A., Simeone, V., 2014. Geomorphometric analysis based on discrete wavelet transform. Environ. Earth Sci. 71, 3095–3108. http://dx.doi.org/10.1007/s12665-013-2686-3.
Foufoula-Georgiou, E., Kumar, P. (Eds.), 1994. Wavelets in Geophysics. Academic Press, New York.
Gagnon, J.S., Lovejoy, S., Schertzer, D., 2006. Multifractal earth topography. Nonlinear Process. Geophys. 13 (5), 541–570.
Gomez, C., 2012. Multi-scale topographic analysis of Merbabu and Merapi volcanoes using wavelet decomposition. Environ. Earth Sci. 67, 1423–1430. http://dx.doi.org/10.1007/s12665-012-1587-1.
Gran, K.B., Belmont, P., Day, S.S., Jennings, C., Johnson, A., Perg, L., Wilcock, P.R., 2009. Geomorphic evolution of the Le Sueur River, Minnesota, USA, and implications for current sediment loading. Geol. Soc. Am. Spec. Pap. 119–130 (Geological Society of America).
Gupta, V.K., Waymire, E., 1989. Statistical self-similarity in river networks parameterized by elevation. Water Resour. Res. 25, 463–476. http://dx.doi.org/10.1029/WR025i003p00463.
Horton, R.E., 1945. Erosional development of streams and their drainage basins: hydrophysical approach to quantitative morphology. Geol. Soc. Am. Bull. 56, 275. http://dx.doi.org/10.1130/0016-7606(1945)56[275:EDOSAT]2.0.CO;2.
Hough, S.E., 1989. On the use of spectral methods for the determination of fractal dimension. Geophys. Res. Lett. 16, 673–676. http://dx.doi.org/10.1029/GL016i007p00673.
Jordan, G., Schott, B., 2005. Application of wavelet analysis to the study of spatial pattern of morphotectonic lineaments in digital terrain models. A case study. Remote Sens. Environ. 94, 31–38. http://dx.doi.org/10.1016/j.rse.2004.08.013.
Kalbermatten, M., Van De Ville, D., Turberg, P., Tuia, D., Joost, S., 2012. Multiscale analysis of geomorphological and geological features in high resolution digital elevation models using the wavelet transform. Geomorphology 138, 352–363. http://dx.doi.org/10.1016/j.geomorph.2011.09.023.
Kirchner, J.W., 1993. Statistical inevitability of Horton's laws and the apparent randomness of stream channel networks. Geology 21, 591. http://dx.doi.org/10.1130/0091-7613(1993)021<0591:SIOHSL>2.3.CO;2.
Kirkby, M.J., 1976. Tests of the random network model, and its application to basin hydrology. Earth Surf. Process. 1, 197–212. http://dx.doi.org/10.1002/esp.3290010302.

Mallat, S.G., 1989a. A theory for multiresolution signal decomposition: the wavelet representation. IEEE Trans. Pattern Anal. Mach. Intell. 11, 674–693. http://dx.doi.org/10.1109/34.192463.

Mallat, S.G., 1989b. Multifrequency channel decompositions of images and wavelet models. IEEE Trans. Acoust. Speech Signal Process. 37, 2091–2110. http://dx.doi.org/10.1109/29.45554.

Nicollet, J.N., 1993. Joseph N. Nicollet on the Plains and Prairies: The Expeditions of 38–39, With Journals, Letters, and Notes on the Dakota Indians. The National Academies.

Ojakangas, R.W., 1982. Minnesota's Geology. University of Minnesota Press.

Orloff, T., Kreslavsky, M., Asphaug, E., 2013. Distribution of polygon characteristic scale in Martian patterned ground terrain in the northern hemisphere using the Fourier transform: Mars patterned ground scale distribution. J. Geophys. Res. Planets 118, 1558–1566. http://dx.doi.org/10.1002/jgre.20111.

Paybins, K.S., 2000. Water quality in the Kanawha-New River Basin: West Virginia, Virginia, and North Carolina, 1996–98. US Geol. Surv. 1204.

Pelletier, J.D., 1999. Self-organization and scaling relationships of evolving river networks. J. Geophys. Res. Solid Earth 104, 7359–7375. http://dx.doi.org/10.1029/1998JB900110.

Perron, J.T., Kirchner, J.W., Dietrich, W.E., 2008. Spectral signatures of characteristic spatial scales and nonfractal structure in landscapes. J. Geophys. Res. 113. http://dx.doi.org/10.1029/2007JF000866.

Rodriguez-Iturbe, I., Rinaldo, A., 2001. Fractal River Basins: Chance and Self-Organization. Cambridge University Press.

Strahler, A.N., 1957. Quantitative analysis of watershed geomorphology. Trans. Am. Geophys. Union 38, 913. http://dx.doi.org/10.1029/TR038i006p00913.

Tarboton, D.G., 1996. Fractal river networks, Horton's laws and Tokunaga cyclicity. J. Hydrol. 187, 105–117. http://dx.doi.org/10.1016/S0022-1694(96)03089-2.

Tokunaga, E., 1978. Consideration on the Composition of Drainage Networks and Their Evolution. 13. Department of Geography, Tokyo Metropolitan Universitypp. 1–27.

Tucker, G.E., Bras, R.L., 1998. Hillslope processes, drainage density, and landscape morphology. Water Resour. Res. 34, 2751–2764. http://dx.doi.org/10.1029/98WR01474.

United Stated Bureau of Reclamation, 2008. Methow Subbasin Geomorphic Assessment, Okanogan County Technical Appendices. Department of the Interior Bureau of Reclamation.

Veneziano, D., Iacobellis, V., 1999. Self-similarity and multifractality of topographic surfaces at basin and subbasin scales. J. Geophys. Res. Solid Earth 104, 12797–12812. http://dx.doi.org/10.1029/1999JB900083.

de Vente, J., Poesen, J., Arabkhedri, M., Verstraeten, G., 2007. The sediment delivery problem revisited. Prog. Phys. Geogr. 31, 155–178. http://dx.doi.org/10.1177/0309133307076485.

Voss, R.F., 1988. Fractals in nature: from characterization to simulation. In: Peitgen, H.-O., Saupe, D. (Eds.), The Science of Fractal Images. Springer New York, New York, NY, pp. 21–70.

Wörman, A., Packman, A.I., Marklund, L., Harvey, J.W., Stone, S.H., 2007. Fractal topography and subsurface water flows from fluvial bedforms to the continental shield. Geophys. Res. Lett. 34. http://dx.doi.org/10.1029/2007GL029426.

Zanardo, S., Zaliapin, I., Foufoula-Georgiou, E., 2013. Are American rivers Tokunaga self-similar? New results on fluvial network topology and its climatic dependence. J. Geophys. Res. Earth Surf. 118, 166–183.